ARTICLE NO. 79-1172R

122
J80-122

Measurements and Model Validation for Composite Propellants Burning under Cross Flow of Gases

20003
60012

Mohan K. Razdan* and Kenneth K. Kuo†
The Pennsylvania State University, University Park, Pa.

Erosive burning rates of three types of ammonium perchlorate-based composite propellant formulations were measured by using the high-speed motion picture method. Experiments were conducted in a test rig designed to develop a well-defined, turbulent boundary layer with a distinct leading edge by the flow of combustion gases over two-dimensional propellant samples. Erosive burning rate correlations which relate the burning rate to freestream velocity and pressure were developed. The comparison of experimental data and theoretical results obtained from the erosive burning model, based upon the turbulent boundary-layer approach developed by the authors, showed a close agreement.

Nomenclature

a = pre-exponent in strand burning rate law, (cm/s) (MPa)$^{-n}$
A_{th} = throat area of exit nozzle, m^2
A_{ts} = cross-sectional flow area in test section, m^2
d_{AP} = average size of AP particles, μm
h_{ts} = height of flow channel above propellant surface, m
H = height of test section without propellant sample, m
K = constant in erosive burning rate correlation, (MPa)$^{-n_p}$(m/s)$^{-n_u}$
n_u = velocity exponent in erosive burning rate correlation
M_{ts} = Mach number in test section
n = pressure exponent in strand burning rate law
n_p = pressure exponent in erosive burning rate correlation
p = pressure, MPa
r_b = $r_{b0} + r_{be}$, total burning rate, cm/s
r_{be} = erosive burning rate, cm/s
r_{b0} = strand burning rate, cm/s
R = gas constant, 437.6 N-m/kg-K
t = time, s
T_0 = stagnation temperature, 2258 K
T_∞ = freestream gas temperature, K
U_{th} = threshold velocity, m/s
U_{ts} = average velocity in test section, m/s
U_∞ = freestream velocity in test section, m/s
x = distance from leading edge along propellant surface, cm
y = location of burning propellant surface, cm
α_1 = constant in erosive burning rate correlation, (cm/s) (m/s)^{n_u} (MPa)$^{-\omega}$
δ = boundary layer thickness, m
η = exponent in boundary layer velocity profile
γ = ratio of constant pressure and constant volume specific heats, 1.26
ω = pressure exponent in Eq. (5)

Presented as Paper 79-1172 at the AIAA/SAE/ASME 15th Joint Propulsion Conference, Las Vegas, Nev., June 18-20, 1979; submitted Sept. 13, 1979; revision received Nov. 26, 1979. Copyright © American Institute of Aeronautics and Astronautics, Inc., 1979. All rights reserved. Reprints of this article may be ordered from AIAA Special Publications, 1290 Avenue of the Americas, New York, N.Y. 10019. Order by Article No. at top of page. Member price $2.00 each, nonmember, $3.00 each. **Remittance must accompany order.**

Index categories: Solid and Hybrid Rocket Engines; Boundary Layers and Convective Heat Transfer—Turbulent.

*Assistant Professor, Dept. of Mechanical Engineering. Member AIAA.

†Associate Professor, Dept. of Mechanical Engineering. Member AIAA.

I. Introduction

THE term "erosive burning" refers to the sensitivity of the solid-propellant burning rate to the velocity of the combustion gases flowing parallel to the propellant surface. The burning rate generally increases with an increase in gas velocity. A high-velocity gas flow usually occurs in the central port of a propellant grain used in a rocket motor. In designing rocket motors, it is essential to be able to predict the burning rate under high cross-flow velocities, since both the thrust level and the web burnout time depend on the burning rate. Erosive burning effect is particularly important in the design of high-thrust, short-burning-time solid-propellant motors for high-acceleration rockets and missiles. Gases in a nozzleless rocket motor choke somewhere within the port, and the gas velocity reaches sonic and supersonic speeds over some portions of the propellant surfaces, leading to high erosive burning rates. In order to have high performance, it is necessary to achieve high-loading fractions (ratio of propellant weight to combustion chamber volume) in a solid-propellant rocket motor. However, with high-loading fractions, erosive burning often results in high-pressure peaks, unequal propellant-web burnout, and extended heat exposure of the chamber wall. Chamber failure may even occur due to overpressurization immediately after ignition, when combustion gas velocity is at maximum. An understanding of the erosive burning characteristics of a solid propellant can lead to the elimination of these problems through proper modifications in the motor and/or grain design.

The literature reviews by Kuo and Razdan[1] and by King[2] indicate that the erosive burning behavior of solid propellants has been investigated in the past by both experimental and theoretical methods. Over the years, a number of models for a possible erosive burning mechanism have been developed to predict the burning rates of solid propellants. These models include: 1) the work of Lenoir and Robillard,[3] based on a heat-transfer theory; 2) Vandenkerckhove's work,[4] based on a flame theory; 3) the flame-bending model of King;[5] and 4) the boundary layer models of Razdan and Kuo,[6] Beddini,[7] and Lengellé.[8] Although there are various approaches to attacking the problem of erosive burning, a realistic approach must consider the burning of the solid propellant under the influence of a boundary layer (mostly turbulent) developed over the propellant surface by the flow of combustion gases.

Experimental studies on erosive burning are important for comparing theoretical predictions and measured erosive burning rates. Erosive burning has been studied experimentally in various ways. The methods used include, for example, partial or interrupted-burner techniques,[9-11]

cineradiography technique,[10] X-ray flash and pressure pick-up methods,[12] conductivity probe technique,[13] and high-speed photography technique.[5,14] None of these experimental studies were designed to be compatible for a boundary layer type of theoretical analysis. Moreover, in most of the previous experimental work, the freestream velocities were limited to low values. In the wake of the recent developments of theoretical models[6-8] based on turbulent boundary-layer approaches, there is a need for erosive burning data for propellants over which turbulent boundary layers are formed. The present experimental approach is unique in that the experiments were conducted in a test rig designed to develop a turbulent boundary layer with a distinct leading edge by the flow of gases over a propellant sample. There is no previous report of erosive burning data under such conditions.

The objectives of the present study were to: 1) conduct erosive burning tests at various pressures and freestream velocities on two-dimensional flat ammonium perchlorate-based composite solid propellant slabs; 2) establish a data base for erosive burning rate as a function of gas velocity, pressure, and propellant physico-chemical characteristics; 3) correlate the erosive burning rate data in terms of freestream velocity and pressure; and 4) use the experimental data for the verification of the theoretical model developed by the authors at the Pennsylvania State University.

II. Experimental Apparatus

A. Erosive Burning Test Rig

The present experiments were designed for verification purposes, so that erosive burning rates measured at various freestream velocities and pressures can be compared with theoretical calculations. Consistent with the theoretical model,[6] the propellant samples in all tests were of flat geometry.

In the design consideration, two requirements were imposed on the structure of the experimental apparatus: 1) experiments should be compatible with the theoretical model;[6] and 2) combustion product gas temperature, pressure, and freestream velocity for burning of a propellant should be similar to that surrounding combustion of a typical solid propellant motor. Therefore, a turbulent boundary layer should be formed over a flat test propellant surface by the flow of a high-velocity gas, and the propellant should burn at typical rocket pressures of 25-100 atm. Various materials and dimensions of the test rig were selected on the basis of a computer-aided design and parametric study, and the requirements of high-pressure and high-temperature gas flow (see Ref. 15 for details). A schematic diagram of the test is shown in Fig. 1. Description and function of each important component is given in the following.

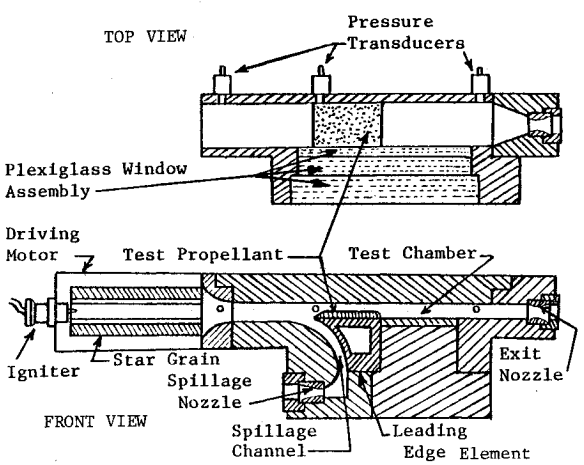

Fig. 1 Schematic diagram of erosive burning test rig.

Driving Motor

A high-pressure, high-velocity, hot combustion gas flow needed to simulate actual rocket conditions was generated in the driving motor by burning a 30-cm long and 11.96-cm outer diameter, 8-point star-shaped N-4 solid-propellant grain. It may be noted here that the flame temperature of the driver propellant grain is different from that of the test propellant samples. Consequently, the freestream temperature in the present experiments was different from the flame temperature of a test propellant. However, this is not believed to affect the results, because the erosive burning rate in previous studies[5,12] was found to be independent of the freestream gas temperature. The neutral burning characteristics of the driver propellant grain helped to maintain a steady-state pressure in the test chamber after a short ignition transient interval. The driving motor was constructed of 304 stainless steel, with a length of 30 cm, an inner diameter of 12 cm, and an outer diameter of 17.8 cm.

Igniter System

To ignite the propellant charge in the driving motor, a pyrotechnic igniter (MK 125 MOD 5) was used. The igniter was held in a stainless steel igniter holder threaded into a flange attached at the head end of the driving motor. The igniter was set off by a remotely controlled ignition circuit, and the power supply was carried to the igniter through an insulated electrode gland feedthrough [Nanmac Corp., Model A-501-Cu(ss)].

Following ignition of the propellant grain, the product gases flow out of the driving motor into the test chamber through a nozzle. This nozzle; constructed of 304 stainless steel, was designed to converge from a square cross section (42.3 cm^2) at the end of the driving motor to a rectangular cross section (17.8 cm^2) at the entrance of a test chamber.

Test Chamber

Several important elements were designed to form the 39-cm long test chamber made of 304 stainless steel with a rectangular cross section 7 cm × 2.54 cm:

1) The test chamber was equipped with a transparent plexiglass window assembly composed of an inner sacrificial plexiglass window (25.4 cm × 3.81 cm × 1.27 cm), a middle window (25.4 cm × 3.81 cm × 2.54 cm), and a top window (27.94 cm × 6.35 cm × 3.81 cm). Rubber O-rings between the middle and top windows were used to insure a tight seal. A new sacrificial window was used in each test firing. The test-propellant sample was clearly visible through the plexiglass window assembly.

2) An interchangeable wedge-shaped stainless steel leading edge was provided, and a test-propellant sample was glued to the top flat surface of the leading edge. The length of the leading edge (10.8 cm) allowed the development of a turbulent boundary layer over a large portion of the propellant sample.

3) A spillage channel was provided. A small amount of the product gases flowed through the channel and out of the test chamber, enabling the boundary layer to develop from the beginning of the leading edge.

4) An interchangeable top plate was designed to vary the channel height in the test section to change gas velocity. Pressure gradient can also be controlled by using a tapered top plate.

5) Convergent-divergent interchangeable exit nozzles made of stainless steel were designed to control the pressure and gas velocity in the test chamber. Various nozzles, with throat diameters of 1.93 cm, 2.08 cm, and 2.42 cm, were used. The exit-nozzle assembly contained a burst diaphragm designed to rupture at a given critical pressure of 30 atm. A small nozzle with a throat diameter of 0.65 cm was used at the end of the spillage channel. To ensure that the spillage channel remained open during the test firing, the burst diaphragm was not used in the small nozzle assembly.

B. Burning Rate Measuring Technique

The high-speed motion picture method was used to determine the burning rate of a test-propellant sample. The burning test propellant was photographed by a 16-mm high-speed motion picture camera (400-ft capacity Hycam Model K20S4E-115). A telescopic lens (Elgeet Rochester Co., 6-in., $f/3.8$, ciné Navitar No. A2305) was also used with the camera. The framing rate of the camera during the experiments was set from 1000 to 1500 frames per second. The camera was equipped with two light-emitting diodes (LED), one for generating timing signals at a preselected frequency and the other for a common-time marker. During the filming of the burning propellant, time marks were recorded on the film, and a common-time mark was also recorded on the film at that time at which ignition was started in a test firing. At the same time, a voltage signal was recorded on a magnetic tape recording system which also recorded pressure-time data at various locations of the test rig. In this way, burning rate vs time data were coordinated with pressure vs time data. The light-emitting diodes were operated by a timing light generator (LED driver), which was fabricated by The Pennsylvania State University Electronics Services and has a frequency range of 10-10,000 Hz. The frequency in the present experiments was set at 100 Hz.

The film was analyzed frame by frame on a motion analyzer, by means of the Vanguard motion analyzer (M-16GD Serial No. 772 projection head, C-11D Serial No. 773 projection case). The motion analyzer projects a 4×-magnified picture on a screen. The screen has two crosshairs which can be moved in x and y directions. The distance moved by these crosshairs is obtained from two micrometer dials accurate to a thousandth of an inch. A frame counter is also provided to record the number of frames moved between readings. The readings taken from the analyzer were the y distances (propellant surface location) at a fixed x location, and the frame counter readings. Readings were taken approximately 100 frames apart. The time interval between each reading was calculated from the number of time marks on the film. To convert the y-dial readings recorded from the magnified image to the actual readings, each y-dial reading was multiplied by a scale factor. The scale factor is defined as the ratio between actual object thickness (measured propellant thickness before ignition in a test firing) to the projected image thickness (y-dial reading of the propellant).

C. Instrumentation

Pressure Measuring Equipment

The pressure measuring system consists of piezo-electric quartz transducers, charge amplifiers, and a recording system. Pressure was measured at three locations: 1) near the inlet to the rectangular convergent nozzle at the exit of the driving motor; 2) near the leading edge; and 3) near the exit nozzle. Three pressure transducers (Kistler Model 601B), with a pressure range up to 1000 atm, were used. These transducers were equipped with water-cooled adapters (Kistler Model 628C), which protected the transducers from excessive heating by the high temperature gases. A silicon-rubber insulation material was used to protect the transducer diaphragms from the hot gases. Transducers were not mounted flush with the inner surface of the test chamber, but were slightly recessed from it to provide additional thermal protection. The charge signal produced by a transducer is proportional to the pressure signal, and it was amplified through a charge amplifier (Kistler Model 504E) and recorded on a tape recorder. Calibrations of pressure measurements were made through the charge amplifiers by applying a DC voltage equal to the transducer sensitivity (picoCoulombs/psi) supplied by the manufacturer. The output of the charge amplifier, which represents the measured pressure in terms of voltage (volts/psi), was then recorded. This calibration procedure was checked periodically by measuring a known pressure (using high pressure nitrogen) with the same transducers as those used in the present experiments.

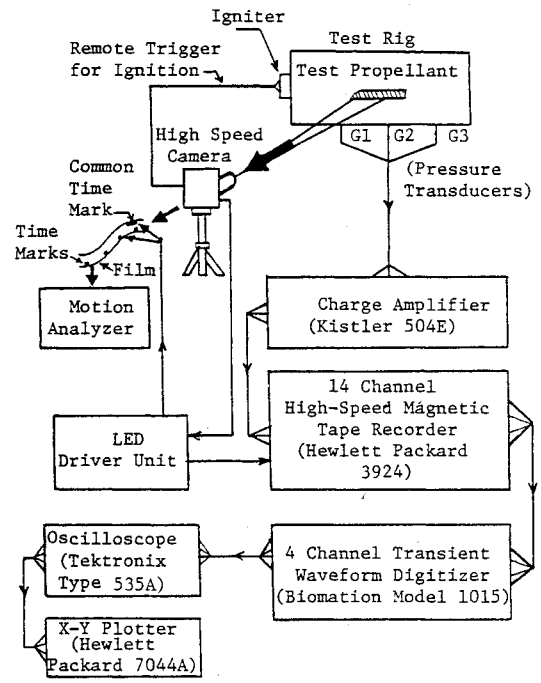

Fig. 2 Schematic diagram of data acquisition system.

Data Acquisition System

Figure 2 illustrates the components of the data acquisition system used in the present erosive-burning experiments. It consists of pressure transducers, charge amplifiers, a 14-channel tape recorder (Hewlett Packard Model 3924 tape system), a 4-channel transient wave form digitizer (Biomation Model 1015), an oscilloscope (Tektronix type 535A), an x-y plotter (Hewlett-Packard 7044A), a high-speed movie camera, an LED driver unit, and a motion analyzer. A pressure transducer produces a small electric charge proportional to the pressure in the test chamber. This charge is carried by an insulated high impedance cable to the charge amplifier, which after amplification converts it into voltage output proportional to the pressure. The output of the charge amplifier is recorded on an FM channel of the tape recorder. Output of the tape recorder is connected to the Biomation digitizer, which converts the data from analog to digital form. The data can be displayed on an oscilloscope, or plotted on the x-y plotter for a hard copy. The burning rate data are obtained through the use of the high-speed motion picture camera and motion analyzer.

D. Procedure Used in Conducting Erosive Burning Test Firings

Before conducting erosive burning test firings, a series of cold flow tests was performed to check the uniformity of the flow out of the rectangular convergent nozzle. Measurements were made with pitotstatic probes at the exit plane of the convergent nozzle. The measured velocity distributions consistently indicated the uniformity of the flow within the potential core over the major portion of the nozzle exit plane. The data also indicted that the nozzle geometry is adequate for providing a two-dimensional flow. During the course of an erosive burning test firing, a number of safety precautions were taken because of the complexity of the test rig setup. A check list prescribing a systematic procedure for setting up each test firing was used. Some of the requisites for preparing a test firing are described below:

1) Internal surfaces of the driving-motor star grain were spread with an igniter paste composed of potassium perchlorate, boron, and titanium mixed in hexane. The ad-

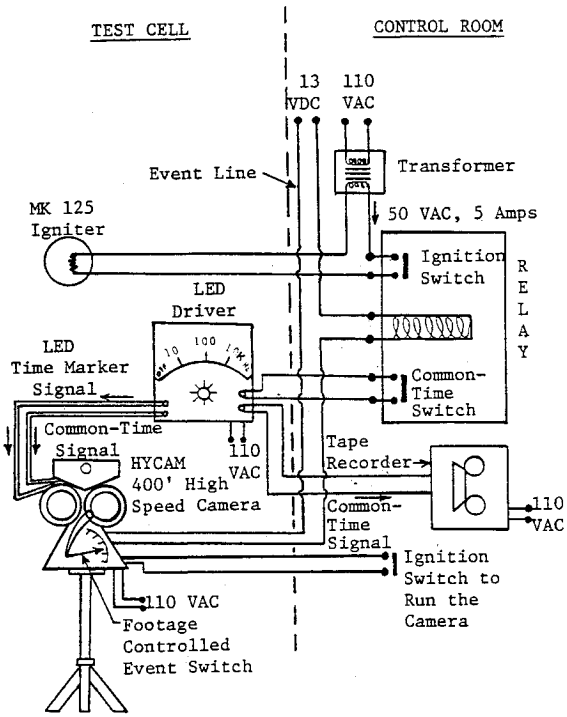

Fig. 3 Circuit diagram for remotely controlled ignition and high-speed photography system.

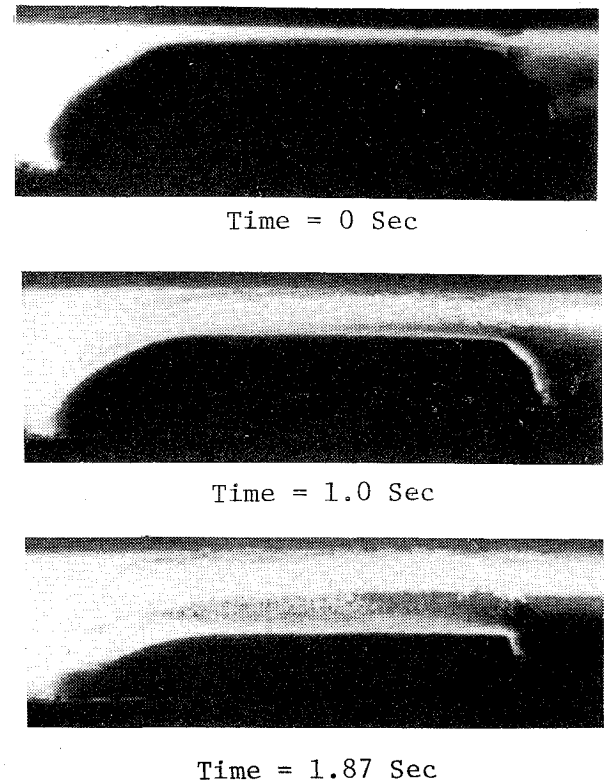

Fig. 4 Photographs showing location of test-propellant surface at various times during a test firing.

vantage of using igniter paste was its ability to spread the flame uniformly and rapidly, thus reducing the time interval of pressurization after ignition.

2) The test propellant was glued to the flat surface of the leading-edge element with an epoxy containing Epon 828 (90%) and diethylene triamine (10%). Normally, 24 h was required for the glue to dry and firmly hold the propellant on the leading edge. Typical test propellant dimensions were length, 10.7 cm; width, 7.3; and thickness, 1.75 cm. The leading-edge portion of the propellant was tapered to ensure smooth development of a boundary layer. The trailing-edge portion of the propellant was also tapered slightly to avoid any flow separation effect in the vicinity of the trailing edge. A little extra width beyond that of the leading-edge width was left for the test propellant sample in each experiment. This was necessary in order to ensure good compression between the sacrificial plexiglass window and the propellant. In this way, no combustion gases could penetrate between the propellant and the plexiglass window.

3) A thin layer of flame retardant (chlorofluorocarbon, Halocarbon 25-5S) was applied to the propellant's front and back surfaces, which were in contact with the plexiglass window and the test chamber wall, respectively. The propellant compression and the use of flame retardant are essential to the experiment in order to prevent flame spreading between the contact surfaces. Flame retardant was also used on the inner surface of the sacrificial plexiglass window to suppress the burning of the window. This helped to obtain a clear view of the burning test propellant sample. In a few of the earlier test firings, it was found that combustion gases generated a small crack in the propellant near the leading edge (stagnation region); eventually, the crack became larger as a result of crack propagation and rapid flame penetration into the crack. A small portion of the propellant leading edge was also covered with the flame retardant layer to avoid development of cracks.

4) The contact surfaces of various components of the test rig were sealed by applying a layer of rubber-based adhesive sealant (Permatex No. 6BR). This was found to be very effective in achieving a good seal.

5) A pre-ignition test was made just before each actual test firing. A fuse wire was used to simulate the igniter, the high-speed movie camera was loaded with a dummy film, and various control switches were then activated in the same sequence as in an actual test firing. If the setup was appropriate, the fuse wire would burn, thus confirming the proper function of the remotely controlled ignition circuit.

6) Four camera lights (two 1000 W and two 650 W) were used to illuminate the window and the propellant in the test chamber.

7) A 16-mm, 200-ft color film was used in each test firing. The film used was Kodak, Eastman Ektrachrome 7250 with ASA 400 (tungsten). The f-stop on the telescopic lens was set at 8.0 for all tests conducted.

Remotely Controlled Ignition System

A circuit diagram for the remotely controlled ignition and high-speed photography system is shown in Fig. 3. Basically, the MK 125 igniter is set off by an event switch built into the high-speed movie camera. When the ignition switch is activated, the camera takes some time to reach a steady preselected framing rate. Corresponding to this time is the length of film which the camera rolls before ignition. Film length is dependent on the selected framing rate (e.g., 30 ft for the present experiments, at about 1500 frames per second) and can be preset with a footage-controlled event switch built into the camera. After the camera runs through the initial film length, the event switch closes, activating a relay switch, and then setting off the igniter.

III. Data Reduction and Analysis

A. Calculation of Burning Rate from Experimental Data

Burning rate data were obtained from the photographic record of a test firing, as discussed in Sec. II.B. Three photographs showing the location of the test-propellant surface during a test firing at various times are shown in Fig. 4. For each y reading, the corresponding time t was computed from the number of time marks on the film. In order to permit accurate computation of first derivatives ($r_b = \mathrm{d}y/\mathrm{d}t$), a least-square polynomial fit through $y \sim t$ data was conducted

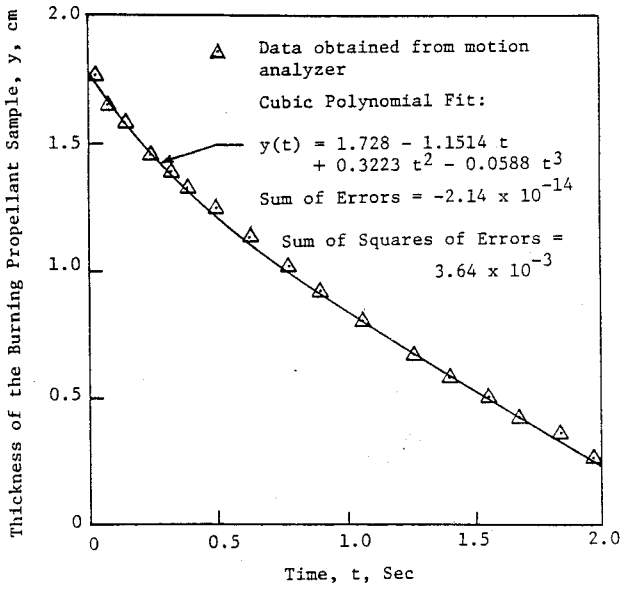

Fig. 5 Least-square polynomial fit to measured y vs t data.

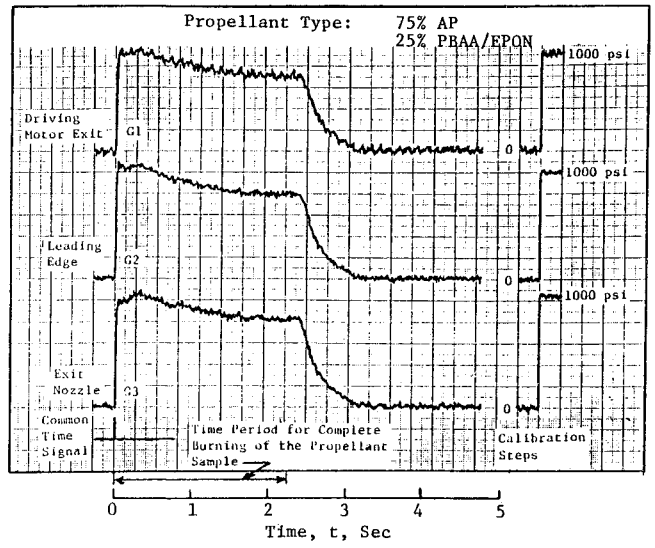

Fig. 6 Measured pressure-time traces in an erosive burning test firing with exit-nozzle throat diameter of 1.93 cm.

to obtain an equation for $y(t)$. Polynomials from the second to the fifth degree were employed, and depending on the least square error, the best fitted polynomial was chosen to represent the data. A typical case is shown in Fig. 5. The sum of squares of errors for this fit was very small (3.64×10^{-3}). The burning rate was calculated by differentiating the polynomial equation with respect to time. In this way, burning rate vs burning time data were obtained from all the test firings. It may be pointed out that the accuracy of the measured burning rate depends on the accuracy of the measurement of the location of the burning propellant surface. Measurements were taken with a motion analyzer capable of measuring line resolution to within 0.001 in. and at an average time interval of 0.01 s. The error introduced in evaluating the burning rate is less than 3%. Because the time marks were put on the film at a precisely known frequency, no error is expected in the calculation of the time interval between film readings.

B. Calculation of Freestream Gas Velocity

Direct measurement of the velocity in the test section is very difficult because of the presence of high-temperature and high-pressure gases. Therefore, the freestream velocity is indirectly calculated from the one-dimensional gas dynamic relationships for flow through a nozzle. Using these relationships and the mass conservation, the average gas velocity in the test section, U_{ts}, was found from the following equation (see Ref. 16):

$$U_{ts} = \left(\frac{A_{th}}{A_{ts}}\right)\sqrt{T_0}\left\{\gamma R\left(\frac{2}{\gamma+1}\right)^{\frac{(\gamma+1)}{(\gamma-1)}}\right\}^{1/2}\left\{1+\frac{\gamma-1}{2}M_{ts}^2\right\}^{1/(\gamma-1)} \tag{1}$$

where A_{ts} is the flow cross-sectional area over the propellant test sample, A_{th} is the throat area of the exit nozzle, and M_{ts} is the average Mach number of the combustion gases in the test section. The Mach number was calculated from the following equation (see Ref. 16):

$$M_{ts} = \left\{\frac{2}{\gamma+1}+\frac{\gamma-1}{\gamma+1}M_{ts}^2\right\}^{\frac{(\gamma+1)}{2(\gamma-1)}}\left(\frac{A_{th}}{A_{ts}}\right) \tag{2}$$

A_{ts} was computed from the product of the width and height h_{ts} of the flow channel above the surface of a test propellant in the test section. This height was obtained from the difference between the height of the test section without propellant sample, H, and the measured location y of the propellant surface. The Mach number in the test section is obtained from Eq. (2), and the average velocity is then calculated from Eq. (1). To obtain an expression for the freestream velocity, correction should be made in the average velocity to account for the boundary layer developed over the propellant surface and the top plate of the test chamber. The freestream velocity was obtained from the following equation:

$$U_\infty = U_{ts}\Big/\left[1+\left(\frac{\eta}{1+\eta}\right)\frac{2\delta}{h_{ts}}\right] \tag{3}$$

where δ is the boundary-layer thickness and η is the exponent in a power-law velocity profile (η was taken as 1/7 in these calculations). Boundary-layer thickness was found from the functional relationship of δ in terms of Reynolds number for a turbulent boundary-layer flow. Equation (3) was developed from a boundary-layer analysis to account for viscous blockage effect in the test section.

C. Erosive-Burning Rate Correlations

Using the measured experimental data, correlations were developed between erosive burning rate augmentation factor (r_b/r_{b0}), freestream velocity, and pressure. The functional form of these correlations was obtained from the experimental data, as explained in the following. The burning rate at a particular pressure is seen to increase somewhat linearly with freestream velocity. An equation relating burning rate and velocity can be written as

$$r_b = r_{b0} + \alpha(U_\infty - U_{th})^{n_u} \tag{4}$$

where U_{th} represents the threshold velocity and α is a constant which must be a function of pressure, since the experimental data indicate that the slope of the r_b vs U_∞ data changes with pressure. Therefore, the following relationship is assumed:

$$\alpha = \alpha_1 p^\omega \tag{5}$$

In this equation α_1 and ω are unknown constants. Although Eq. (4) contains the threshold velocity consideration, our experimental data for all three propellants tested showed no threshold effect. The threshold velocity is retained in Eq. (4) to maintain the generality of the form of the correlation.

From the graphical plot of experimental data for r_b vs U_∞ at three different pressures, approximate values for the

Table 1 Propellant data

Propellant type	I (4525)	II (5051)	III
Composition	AP/HTPB	AP/HTPB	AP/PBAA-EPON
Average particle size, μm	20	200	76
Weight percent of oxidizer	73	73	75
Pre-exponent a in the strand burning rate law, (cm/s) (MPa)$^{-n}$	0.305	0.2026	0.2452
Pressure exponent n in the strand burning rate law	0.5611	0.5427	0.41
Flame temperature of propellant gas, K	1667	1667	1920
Propellant density, kg/m^3	1492	1492	1600

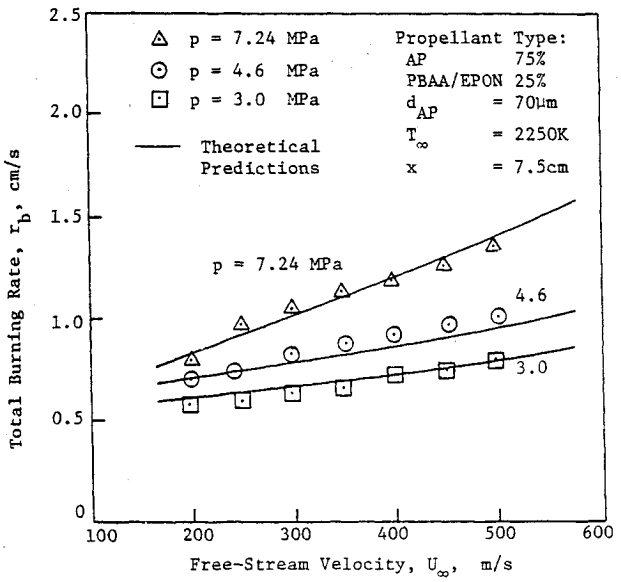

Fig. 7 Comparison of predicted burning rates with experimental data at various pressures and freestream velocities for propellant III.

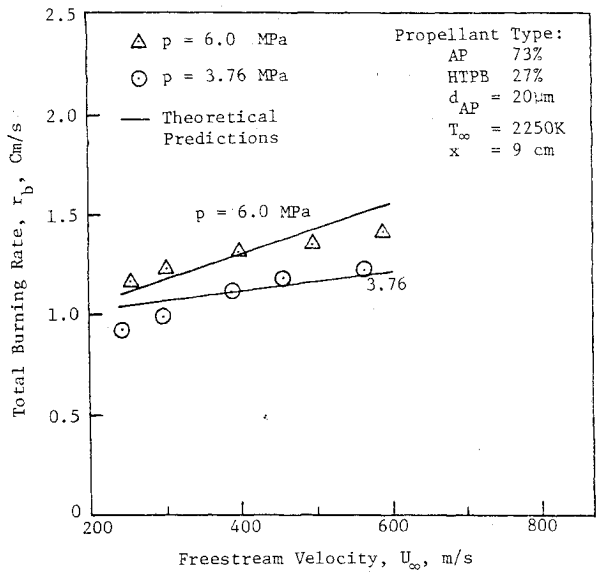

Fig. 8 Comparison of predicted burning rates with experimental data at various pressures and freestream velocities for propellant I.

constants α_1, ω, and n_u were obtained. The values of the approximate constants were then optimized by a regression analysis of the experimental data for the burning rate, freestream velocity, and pressure. The regression analysis was performed with the NLIN2 computer program[17] of the Share Program Library. The model supplied to the NLIN2 program was represented by the following correlation:

$$r_{b_e} = \alpha_1 p^{\omega} (U_\infty - U_{th})^{n_u} \tag{6}$$

This equation is obtained from Eqs. (4) and (5), while r_{b_e} is the erosive burning rate component of the total burning rate r_b of a solid propellant. Using the strand burning rate law ($r_{b_0} = ap^n$) and Eqs. (4) and (5), the correlation represented by Eq. (6) can be written in the following convenient form:

$$(r_b/r_{b_0}) = 1 + Kp^{n_p} (U_\infty - U_{th})^{n_u} \tag{7}$$

The correlation given by Eq. (7) represents, within limits of available data, the effect of freestream velocity and pressure on the burning rate of the solid composite propellants studied. The correlation equation can be represented by a 45 deg line on a r_b/r_{b_0} vs $1 + Kp^{n_p} p (U_\infty - U_{th})^{n_u}$ plot. These plots are discussed in the following section.

IV. Results and Discussion

Figure 6 shows a typical pressure-time trace recorded during a test firing with an exit nozzle throat diameter of 1.93 cm. Several observations can be made from the pressure-time traces:

1) The pressure variation between the peak pressure and the start of the tail-off region is not significant, and the mean flow in the boundary layer can be considered as quasi-steady at any particular time.

2) In all the erosive burning experiments conducted, the time period for a test propellant sample to consume completely was within the time interval during which the chamber was pressurized. The flame-spreading time for the star grain in the driving motor was very short, as can be seen from the sharp pressurization following immediately after the onset of ignition. Therefore, most of the burning time of the star grain was adequately utilized during the test run.

3) The common-time signal shown in Fig. 6 represents that instant at which remotely controlled ignition takes place. This time always coincides with the first discernible pressure rise in the test rig.

Erosive burning characteristics of three types of AP-based composite solid propellants were studied. These propellants and their data are listed in Table 1. Propellants designated by I and II are the same as those used by King[5] in his study (propellant numbers 4525 and 5051 in Table 1 correspond to King's formulation numbers). While propellants I and II have the same binder (HTPB) and oxidizer-to-fuel ratio (73:27), their AP particle size is quite different: 20 μm for propellant I and 200 μm for propellant II. Pressure and velocity ranges covered in the present study were 2 to 7 MPa for pressure, and 200 to 700 m/s for freestream velocity.

Experimental results obtained for AP/PBAA-EPON propellant are plotted in Fig. 7, which shows the variation of total burning rate with freestream velocity at pressures of 7.24, 4.6 and 3.0 MPa. As expected, the burning rate increases with the increase in both pressure and freestream velocity. The slope of the burning rate vs velocity curves decreases with the decrease in pressure. At the same time, the

burning rate at lower pressure changes very slowly at low velocities (close to 200 m/s). Calculated results from the turbulent boundary layer model[6] developed by authors are also plotted in Fig. 7. The agreement between the predicted and measured burning rates is quite close for all pressure considered.

For AP/HTPB propellants, Figs. 8 and 9 show the variation of the measured burning rate with freestream velocity at different pressures. The comparison between the results shown in Figs. 8 and 9 indicates a noticeable difference in the burning behavior of the two propellants with identical ingredients, but with different oxidizer particle sizes. The erosive effect is more pronounced for propellant II with larger particle size, since the gradient of r_b vs U_∞ in Fig. 9 is steeper

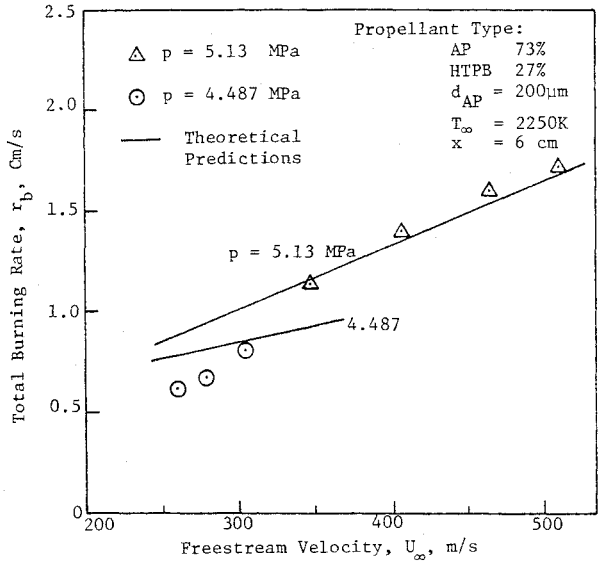

Fig. 9 Comparison of predicted burning rates with experimental data at various pressures and freestream velocities for propellant II.

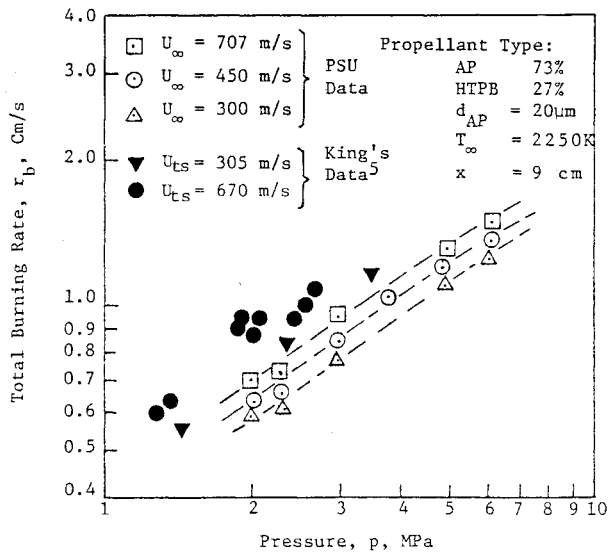

Fig. 10 Measured burning rate vs pressure data for different freestream velocities.

than that in Fig. 8. It is believed that the higher erosive burning rates for propellants with large particles is caused by the roughness effect of the propellant surface. The roughness increases the turbulence activity near a propellant surface, thereby increasing the gas-to-solid heat flux and the burning rate of a propellant. As the particle size increases, the height of the roughness also increases, as does the burning rate of a propellant. This phenomenon is in agreement with the predictions of the turbulent boundary-layer model[6] developed at The Pennsylvania State University. The predictions for propellants I and II are shown as solid lines in Figs. 8 and 9, respectively. The agreement between the theoretical and experimental results is generally good. The surface roughness height of 35% of the AP particle size was used in theoretical calculations. This value of roughness height was obtained by systematically varying the roughness height until the predictions matched the measured burning rate of a propellant. At the same time, all other physical and chemical input data of the propellant were held constant in theoretical calculations. Because of the lack of experimental data for surface roughness, the above procedure of including the surface roughness effect in the theoretical calculations is believed to be reasonable.

It may be noted that the strand burning behavior of the two AP/HTPB propellants is also different as a result of differing particle sizes. Propellant I with 20μ AP has a higher strand burning rate r_{b_o} than propellant II with 200μ AP. For example, at a pressure of 4 MPa, the strand burning rate of propellant I is 0.664 cm/s and that of propellant II is 0.43 cm/s. Previous studies[5,9,12] have found that the strand burning rate of a propellant affects its erosive burning behavior. The present study shows that at a particular velocity, propellant II with lower strand burning rate is more sensitive to the erosive burning effect (see Fig. 9) than is propellant I, with higher strand burning rate. The higher erosive effect for propellant II compared to that of propellant I is believed to be caused by both the larger AP particle size and the lower strand burning rate of the propellant. The effect of strand burning rate on the erosive burning response of a propellant is also predicted by the turbulent boundary layer model.[6]

Measured burning rates for propellant I are plotted against pressure in Fig. 10. This plot was constructed so that a comparison could be made with King's data.[5] King has represented most of his data on r_b vs p plots. A set of data points for different freestream velocities is shown in Fig. 10. The data points from King's work at an average test-section velocity of 305 m/s do not compare well with the data obtained from the present study at a freestream velocity of about 300 m/s. A possible reason for the discrepancy could be that the data reduction procedure used by King is quite different from that used in this study. It was found in our study that the error in reading the instantaneous web thickness from the motion pictures could affect results significantly. Care was taken, with repeated film readings, to measure the web thickness with an accurate motion analyzer. Only a few data points are plotted in Fig. 10, owing to the difficulty of finding a larger number of data points for the burning rate at various pressures while at the same time keeping the freestream velocity constant.

Using the present erosive burning data, correlations similar to Eq. (7) were developed. The correlation coefficients for the three types of propellants investigated are listed in Table 2. It is noted that the functional form of Eq. (7) does not have the

Table 2 Correlation coefficients

Propellant type	I	II	III
K, $(\mathrm{MPa})^{-n_p}(\mathrm{m/s})^{-n_u}$	4.8×10^{-3}	3.167×10^{-4}	2×10^{-4}
n_p	0.35	1.463	0.705
n_u	0.69	1.42	1.252

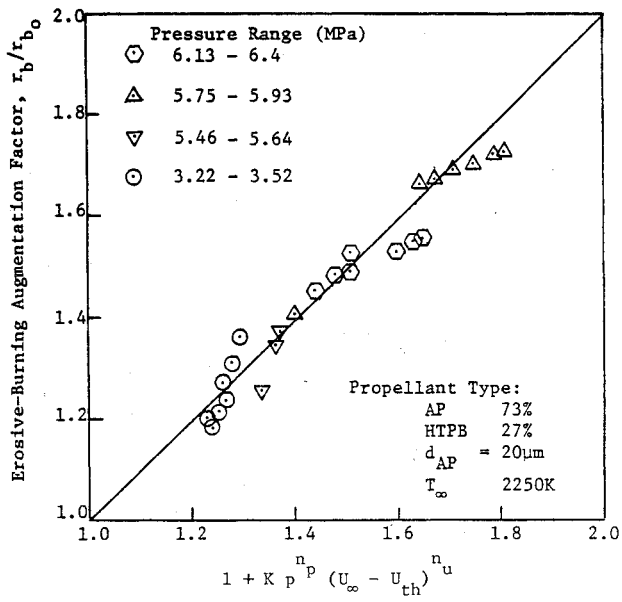

Fig. 11 Experimental data for erosive burning augmentation factor correlated with pressure and freestream velocity for propellant I.

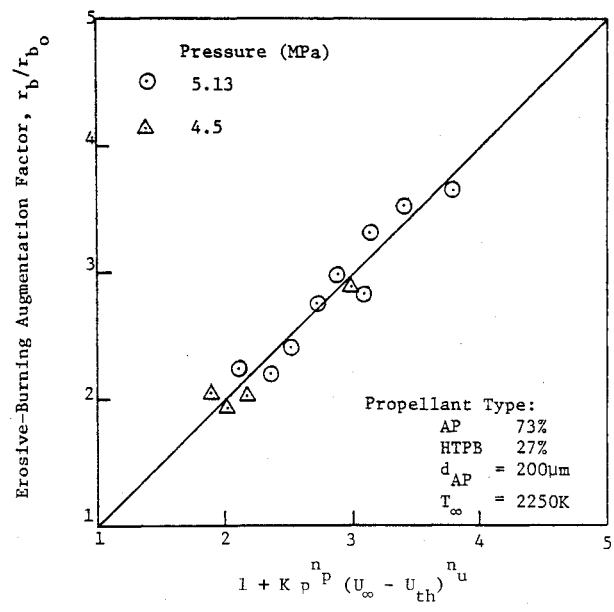

Fig. 12 Experimental data for erosive burning augmentation factor correlated with pressure and freestream velocity for propellant II.

dependence of erosive burning augmentation ratio r_b/r_{b0} on streamwise distance x. The burning rate was measured at three locations ($x = 3$ cm, 6 cm, and 9 cm) along the test propellant surface. A study of the data did not reveal any significant variation of the burning rate along the x direction. This observation was also made by viewing movies of the test firings in which the propellant surface remained horizontal as it burnt downwards. It is believed that the insignificant x-dependence of the burning rate is due to the fact that mass flow rate of gases over the test propellant samples in the experiments remained nearly constant. Contribution from a burning propellant sample mass flow rate was small in all experiments, typically about 6%. It is known from previous studies[9,10] that the erosive burning rate of a solid propellant is strongly influenced by the mass flow rate of gases over the propellant surface. Therefore, with the gaseous mass flow rate nearly constant along the x coordinate, the change in burning rate is also insignificant.

The comparison of experimental data with erosive correlations for propellants I, II, and III are shown in Figs.

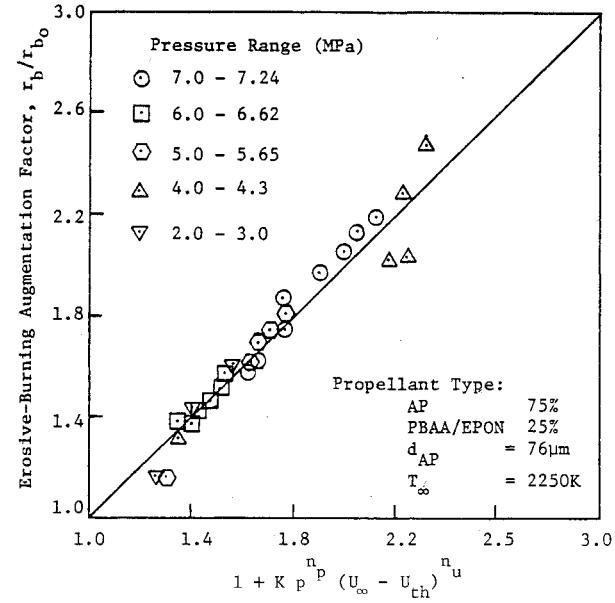

Fig. 13 Experimental data for erosive burning augmentation factor correlated with pressure and freestream velocity for propellant III.

11-13, respectively. Most of the data points are very close to the 45 deg line on these plots. The results of Figs. 11-13 indicate that the correlation given in the form of Eq. (7) is suitable to represent the erosive burning rate data obtained for the three types of composite propellants studied. Such correlations can be used conveniently in the design considerations of a solid propellant rocket motor. The form of the correlations may serve as a guide for other types of composite propellants for which similar correlations can be developed.

V. Summary and Conclusions

An experimental apparatus for measuring the erosive burning rates of solid propellants under wide ranges of pressures and freestream velocities was designed and fabricated. The erosive burning behavior of three types of composite solid propellants was studied by burning test propellant slabs in turbulent boundary layers formed by the flow of hot combustion gases over the propellant samples. The burning rates at various pressures and freestream velocities were measured by a high-speed motion picture technique in which the burning propellant surface was photographed during test firing. The following observations and conclusions can be made from the present study:

1) The predicted results show that propellants with lower strand burning rates are more sensitive to erosive burning than those with higher strand burning rates.

2) The erosive burning effect becomes more pronounced when the oxidizer particle size of a composite propellant is increased.

3) The erosive burning rate correlates well with chamber pressure and freestream velocity. Correlations were developed from the measured burning rate data. Correlations of this type can be used in design considerations of a solid-propellant rocket motor.

4) The experimental data are in close agreement with predicted results obtained from the erosive burning model (based on the turbulent boundary layer approach) developed by the authors.

Acknowledgment

This report represents a part of the results of the research work performed under a subcontract from the Atlantic Research Corporation, the prime contractor for the Air Force Office of Scientific Research (Contract No. F49620-78-C-0016), under the management of Capt. R. F. Sperlein. The

authors would like to acknowledge the processing of propellant samples arranged by D. George at AFRPL and by M. K. King at Atlantic Reserach Corporation. The assistance of R. L. Kovalcin, W. D. Jones, S. M. Kovacic, F. X. White, and J. G. Siefert of The Pennsylvania State University is also acknowledged.

References

[1] Kuo, K. K. and Razdan, M. K., "Review of Erosive Burning of Solid Propellants," *12th JANNAF Combustion Meeting*, CPIA Publication 273, Vol. 2, 1975, pp. 323-338.

[2] King, M. K., "Review of Erosive Burning Models," JANNAF Workshop on Erosive Burning/Velocity Coupling, Lancaster, Calif., March 7-8, 1977.

[3] Lenoir, J. M. and Robillard, G., "A Mathematical Method to Predict the Effects of Erosive Burning in Solid-Propellant Rockets," *Sixth Symposium (International) on Combustion*, Reinhold, New York, 1957, pp. 663-667.

[4] Vandenkerckhove, J. A., "Erosive Burning of a Colloidal Solid Propellant," *Jet Propulsion*, Vol. 28, Sept. 1958, pp. 599-603.

[5] King, M. K., "Erosive Burning of Composite Solid Propellants: Experimental and Modeling Studies," *Journal of Spacecraft and Rockets*, Vol. 16, May-June 1979, pp. 154-162.

[6] Razdan, M. K. and Kuo, K. K., "Erosive Burning Study of Composite Solid Propellants by Turbulent Boundary-Layer Approach," *AIAA Journal*, Vol. 17, Nov. 1979, pp. 1225-1233.

[7] Beddini, R., "Reacting Turbulent Boundary-Layer Approach to Solid Propellant Erosive Burning," *AIAA Journal*, Vol. 16, Sept. 1978, pp. 898-905.

[8] Lengellé, G., "Model Describing the Erosive Combustion and Velocity Response of Composite Propellants," *AIAA Journal*, Vol. 13, March 1975, pp. 315-322.

[9] Green, L., Jr., "Erosive Burning of Some Composite Solid Propellants," *Jet Propulsion*, Vol. 24, Jan.-Feb. 1954, pp. 9-15.

[10] Kreidler, J. W., "Erosive Burning: New Experimental Techniques and Methods of Analysis," AIAA Paper 64-155, Palo Alto, Calif., Jan. 1964.

[11] Peretz, A., "Investigation of the Erosive Burning of Solid-Propellant Grains with Variable Port Area by Means of Interrupted Burning Experiments," *AIAA Journal*, Vol. 6, May 1967, pp. 910-912.

[12] Marklund, T. and Lake, A., "Experimental Investigation of Propellant Erosion," *ARS Journal*, Vol. 3, Feb. 1960, pp. 173-178.

[13] Dickinson, L. A., Jackson, F., and Odgers, A. L., "Erosive Burning of Polyurethane Propellants in Rocket Engines," *Eighth Symposium (International) on Combustion*, Williams and Wilkins, Baltimore, 1962, pp. 754-759.

[14] Zucrow, M. J., Osborn, J. R., and Murphy, J. M., "An Experimental Investigation of the Erosive Burning Characteristics on a Non-Homogeneous Solid Propellant," AIAA Paper 64-107, Palo Alto, Calif., Jan. 29-31, 1964.

[15] Razdan, M. K., and Kuo, K. K., "Erosive Burning Studies of Composite Solid Propellants by the Reacting Turbulent Boundary-Layer Approach," AFOSR-TR-79-1155, Scientific Report to U.S. Air Force Office of Scientific Research, March 1979.

[16] Shapiro, A. H., *The Dynamics and Thermodynamics of Compressible Fluid Flow*, Vol. 1, Ronald Press, New York, 1953, pp. 83-95.

[17] Marquardt, D. W., "Least Square Estimation of Nonlinear Parameters," Engineering Dept., E. I. DuPont de Nemours and Co., Inc., Share Distribution No. 3094, 1965.

From the AIAA Progress in Astronautics and Aeronautics Series . . .

REMOTE SENSING OF EARTH FROM SPACE: ROLE OF "SMART SENSORS"—v. 67

Edited by Roger A. Breckenridge, NASA Langley Research Center

The technology of remote sensing of Earth from orbiting spacecraft has advanced rapidly from the time two decades ago when the first Earth satellites returned simple radio transmissions and simple photographic information to Earth receivers. The advance has been largely the result of greatly improved detection sensitivity, signal discrimination, and response time of the sensors, as well as the introduction of new and diverse sensors for different physical and chemical functions. But the systems for such remote sensing have until now remained essentially unaltered: raw signals are radioed to ground receivers where the electrical quantities are recorded, converted, zero-adjusted, computed, and tabulated by specially designed electronic apparatus and large main-frame computers. The recent emergence of efficient detector arrays, microprocessors, integrated electronics, and specialized computer circuitry has sparked a revolution in sensor system technology, the so-called smart sensor. By incorporating many or all of the processing functions within the sensor device itself, a smart sensor can, with greater versatility, extract much more useful information from the received physical signals than a simple sensor, and it can handle a much larger volume of data. Smart sensor systems are expected to find application for remote data collection not only in spacecraft but in terrestrial systems as well, in order to circumvent the cumbersome methods associated with limited on-site sensing.

505 pp., 6×9, illus., $22.00 Mem., $42.50 List

TO ORDER WRITE: Publications Dept., AIAA, 1290 Avenue of the Americas, New York, N. Y. 10019